Forensic Toxicol (2017) 35:333–347
DOI 10.1007/s11419-017-0361-1

ORIGINAL ARTICLE

In vitro and in vivo pharmacokinetics and metabolism of synthetic cannabinoids CUMYL-PICA and 5F-CUMYL-PICA

Richard C. Kevin[1,2] · Timothy W. Lefever[3] · Rodney W. Snyder[3] · Purvi R. Patel[3] · Timothy R. Fennell[3] · Jenny L. Wiley[3] · Iain S. McGregor[1,2] · Brian F. Thomas[3]

Received: 23 January 2017 / Accepted: 28 February 2017 / Published online: 10 March 2017

Abstract CUMYL-PICA [1-pentyl-*N*-(2-phenylpropan-2-yl)-1*H*-indole-3-carboxamide] and 5F-CUMYL-PICA [1-(5-fluoropentyl)-*N*-(2-phenylpropan-2-yl)-1*H*-indole-3-carboxamide] are recently identified recreationally used/abused synthetic cannabinoids, but have uncharacterized pharmacokinetic profiles and metabolic processes. This study characterized clearance and metabolism of these compounds by human and rat liver microsomes and hepatocytes, and then compared these parameters with in vivo rat plasma and urine sampling. It also evaluated hypothermia, a characteristic cannabimimetic effect. Incubation of CUMYL-PICA and 5F-CUMYL-PICA with rat and human liver microsomes suggested rapid metabolic clearance, but in vivo metabolism was prolonged, such that parent compounds remained detectable in rat plasma 24 h post-dosing. At 3 mg/kg (intraperitoneally), both compounds produced moderate hypothermic effects. Twenty-eight metabolites were tentatively identified for CUMYL-PICA and, coincidentally, 28 metabolites for 5F-CUMYL-PICA, primarily consisting of phase I oxidative transformations and phase II glucuronidation. The primary metabolic pathways for both compounds resulted in the formation of identical metabolites following terminal hydroxylation or dealkylation of the *N*-pentyl chain for CUMYL-PICA or of the 5-fluoropentyl chain for 5F-CUMYL-PICA. These data provide evidence that in vivo elimination of CUMYL-PICA, 5F-CUMYL-PICA and other synthetic cannabinoids is delayed compared to in vitro modeling, possibly due to sequestration into adipose tissue. Additionally, the present data underscore the need for careful selection of metabolites as analytical targets to distinguish between closely related synthetic cannabinoids in forensic settings.

Keywords Synthetic cannabinoid · Pharmacokinetics · Metabolism · CUMYL-PICA · 5F-CUMYL-PICA · Delayed clearance in vivo

Introduction

Synthetic cannabinoid receptor 1 (CB_1) agonists comprise a large and growing class of recreationally used novel psychoactive substances. These synthetic chemicals produce psychoactive "cannabimimetic" effects in humans and rodents [1–5], and their use as recreational drugs has been linked to a number of adverse health effects [6–9]. The molecular structures of these compounds are regularly altered in an attempt to evade drug detection and legislation [10], and consequently users of synthetic cannabinoids are frequently exposed to novel substances with unknown pharmacokinetic and pharmacodynamic properties.

Two such novel synthetic cannabinoids are CUMYL-PICA [1-pentyl-*N*-(2-phenylpropan-2-yl)-1*H*-indole-3-carboxamide] and its fluorinated analogue 5F-CUMYL-PICA [1-(5-fluoropentyl)-*N*-(2-phenylpropan-2-yl)-1*H*-indole-3-carboxamide]. These synthetic cannabinoids are α,α-dimethylbenzyl analogues of SDB-006 and 5F-SDB-006, which are in turn analogues of SDB-001 (APICA) and STS-135 (Fig. 1). They are also structurally related to a

✉ Richard C. Kevin
richard.kevin@sydney.edu.au

[1] School of Psychology, The University of Sydney, A18, Sydney, NSW 2006, Australia

[2] The Lambert Initiative for Cannabinoid Therapeutics, The University of Sydney, Sydney, NSW 2050, Australia

[3] RTI International, 3040 Cornwallis Road, Research Triangle Park, Durham, NC 27709, USA

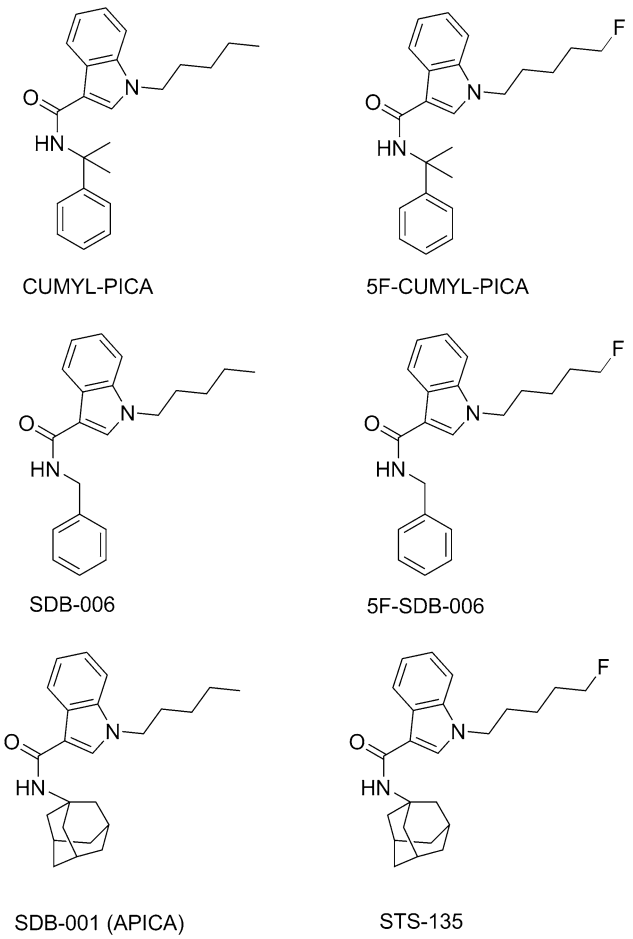

Fig. 1 Structures of CUMYL-PICA and 5F-CUMYL-PICA compared to benzyl analogues SDB-006 and 5F-SDB-006 and to adamantyl analogues SDB-001 and STS-135

number of other carboxamide synthetic cannabinoids such as AMB and 5F-AMB. CUMYL-PICA was detected first in European synthetic cannabinoid products in 2014 [11], and 5F-CUMYL-PICA was recently detected in toxicological analyses of blood samples in Germany [12].

To our knowledge, the pharmacokinetics of CUMYL-PICA and 5F-CUMYL-PICA have not been characterized. A thorough understanding of these processes is important for determining drug toxicology and for identifying these compounds in biological matrices where they are likely extensively metabolized [13–15]. A precise understanding of metabolic pathways is necessary, because closely structurally related synthetic cannabinoids can produce identical metabolites, which can increase the difficulty of forensic identification of a unique compound [13, 15]. In addition, some synthetic cannabinoid metabolites retain cannabinoid receptor efficacy and therefore may be relevant to the overall pharmacological profile following drug administration [16, 17].

Thus, the present study aimed to characterize the pharmacokinetics related to metabolism and clearance of CUMYL-PICA and 5F-CUMYL-PICA. First, these compounds were assessed in vitro using rat and human liver microsomes and hepatocytes, in order to measure clearance and to establish metabolic pathways. These assays were followed by in vivo kinetic assessment in rat blood and urine sampled at several time points following drug administration and measurement of body temperature. These data were used to propose metabolic pathways for CUMYL-PICA and 5F-CUMYL-PICA in rats and humans, to examine the predictive utility of in vitro approaches to synthetic cannabinoid metabolic studies, and to suggest viable analytical targets for forensic analysis.

Materials and methods

Chemicals and reagents

CUMYL-PICA and 5F-CUMYL-PICA were obtained from Cayman Chemicals (Ann Arbor, MI, USA). Acetonitrile and formic acid were purchased from Fisher Scientific (Raleigh, NC, USA). Rat and human liver microsomes and hepatocytes were obtained from XenoTech (Kansas City, KS, USA). Polysorbate 80 was purchased from Fisher Scientific (Pittsburgh, PA, USA) and saline from Patterson Veterinary Supply (Devens, MA, USA). All chemicals and solvents were at least ACS or high-performance liquid chromatography grade, respectively.

In vitro incubations

Rat and human liver microsomes

CUMYL-PICA and 5F-CUMYL-PICA were incubated at 1 μM with male human (pooled) or rat (pooled IGS Sprague–Dawley) liver microsomes at 37 °C, in triplicate, with gentle shaking. A solution of each compound was prepared in acetonitrile at a concentration of 0.1 mM. An assay mixture containing microsomes (1 mg protein/mL final concentration), nicotinamide adenine dinucleotide phosphate reduced form (NADPH; 1 mM final) and a buffer consisting of 50 mM potassium phosphate buffer, pH 7.4, with 3 mM $MgCl_2$ was prepared and pre-incubated at 37 °C for 5 min. Ten microliters of the 0.1 mM drug solutions was added to 990 μL of assay mixture in a glass test tube in a 37 °C water bath to initiate the assay; 100-μL samples were removed at 0, 5, 10, 30, and 60 min and added to 100 μL acetonitrile. Samples were centrifuged and stored at −80 °C until analysis.

Rat and human hepatocytes

Incubation of CUMYL-PICA and 5F-CUMYL-PICA at 10 μM with male human or rat hepatocytes was performed in triplicate, with 1 mL cell suspension (rat: 0.86×10^6 cells/mL, 80% viability; human: 0.80×10^6 cells/mL, 81.6% viability) in 24-well polystyrene cell culture plates in a 37 °C incubator with 5% CO_2 atmosphere. Both compounds were formulated in acetonitrile at 10 mM and further diluted to 1 mM in acetonitrile so that the final concentration of acetonitrile in the incubation was 1% after the addition of 10 μL drug solution to 990 μL of hepatocyte suspension. Incubation was conducted simultaneously using 1 mL incubation cell blank containing live cells and solvent blank; this incubation was treated exactly as the cell incubations. At 0, 10, 60, and 180 min, a 100-μL sample was removed and terminated with 100 μL acetonitrile, vortexed (11,000 *g* for 1 min) and stored at −80 °C until analysis.

In vivo dosing and sampling in rats

Animals

Twelve 49-day-old male Long–Evans rats (226.8–286.7 g) with jugular vein catheters were purchased from Charles River Laboratories (Raleigh, NC, USA). Different groups of rats ($n = 4$ per group) were used to test each compound and vehicle control. Prior to testing, all animals were kept in a temperature-controlled environment (20–22 °C) on a 12-h light–dark cycle (lights on at 6 a.m.), with access to food and water ad libitum. All in vivo work was carried out in accordance with guidelines published in the Guide for the Care and Use of Laboratory Animals (National Research Council 2011), and were approved by the RTI International Institutional Animal Care and Use Committee.

Procedures

The animals were placed individually into glass metabolic cages (Prism Research Glass, Raleigh, NC, USA). Animals were administered intraperitoneal injections, in case of 3 mg/mL CUMYL-PICA or 3 mg/mL 5F-CUMYL-PICA dissolved in vehicle solution comprising 7.8% polysorbate 80 NF (Fisher Scientific, Pittsburgh, PA, USA) and 92.2% saline USP (Patterson Veterinary Supply, Devens, MA, USA), with an injection volume of 1 mL/kg of rat body weight. Blood samples (200 μL) were drawn 15 min pre-injection and 15 min, 30 min, 1 h, 2 h, 4 h, 8 h, and 24 h post-injection, put into chilled K_3EDTA collection tubes, and centrifuged at 2800 *g* for 10 min at 4 °C. The plasma supernatant was decanted and stored at −80 °C until further analysis. Rectal temperature was also recorded at these time points using a digital thermometer (Physitemp Instruments Inc., Clifton, NJ, USA). Urine was collected at 8 and 24 h post-injection. At 24 h post-injection, rats were euthanized via CO_2 asphyxiation, and blood was rapidly collected and stored as specified above.

Analyte extraction

Extractions of all analytes (parent compounds and metabolites) from all matrices (microsomes, hepatocytes, plasma, and urine) was performed as follows. Acetonitrile was added in a 3:1 ratio to the sample volume (microsomes/hepatocytes sample volume 50 μL; plasma 25 μL; urine 100 μL) and centrifuged at 4000 *g* for 15 min at 4 °C. Supernatants were transferred to vials for immediate analysis via liquid chromatography–tandem mass spectroscopy (LC–MS/MS).

LC–MS/MS analyses

Parent compounds CUMYL-PICA and 5F-CUMYL-PICA in the media following incubation with rat and human liver microsomes and in rat plasma were quantified using LC–MS/MS. The LC–MS/MS system consisted of a Waters Acquity UPLC system, equipped with a Waters BEH C18 column (100 mm × 2.1 mm i.d., particle size 1.7 μm; Waters Corp., Milford, MA, USA), coupled to an API 5000 tandem mass spectrometer (AB Sciex, Framingham, MA, USA). Gradient elution was used with mobile phase solutions 0.1% formic acid in water (A) and acetonitrile (B), which started at 10% B for 0.5 min and was then ramped to 95% B over 10 min, held until 12.5 min and then returned to 10% B for 2.5 min, with a total run time of 15 min. The mass spectrometer was operated in positive electrospray ionization mode with multiple reaction monitoring. The monitored transitions were *m/z* 349.1 → 231.1 for CUMYL-PICA and *m/z* 367.1 → 249.1 for 5F-CUMYL-PICA.

Metabolites were also identified using LC–MS/MS, with a Thermo Fisher LTQ Orbitrap Velos mass spectrometer (Thermo Fisher Scientific, Waltham, MA, USA) coupled to a Waters Acquity UPLC system (Waters Corp.). Chromatographic conditions were identical to those specified above. The mass spectrometer was operated in positive electrospray ionization mode, with scan range of *m/z* 100–910 and capillary temperature of 250 °C. Because during method development, poor fragmentation was observed across a range of collision energies, higher-energy collisional dissociation was implemented, with a collision energy at 35 eV.

Data analysis

Hypothermic effects were statistically analyzed using a two-factor mixed ANOVA with drug treatment (vehicle, 3 mg/kg CUMYL-PICA, or 3 mg/kg 5F-CUMYL-PICA) as the between-subject factor and time (pre-dose, 15 min, 30 min, 1 h, 2 h, 4 h, 8 h, and 24 h) as the within-subject factor. Simple effects of drug treatment were then analyzed using Dunnett's tests ($\alpha = 0.05$), which compared the CUMYL-PICA or 5F-CUMYL-PICA cohort to the vehicle cohort at each time point.

Microsomal intrinsic clearance ($CL_{int,micr}$) and half-life were calculated from plots of chromatographic peak areas against time. Intrinsic clearance (CL_{int}) was calculated by scaling $CL_{int,micr}$ to whole-liver dimensions for rats and humans [18, 19]. Hepatic clearance (CL_H) and extraction ratios (ER) were estimated based on the corresponding rat and human CL_{int} values and estimates of liver blood flow rate (rat 13.8 mL/min; human 1400 mL/min) [20]. Plasma concentrations of CUMYL-PICA and 5F-CUMYL-PICA were calculated via a standard curve of the corresponding calibrator samples using a reference standard. Plasma kinetic parameters were then computed from plasma concentrations of each compound via non-compartmental analysis performed with WinNonlin® (Certara, Princeton, NJ, USA).

Metabolites were identified in hepatocyte incubations, rat plasma, and rat urine using Compound Discoverer 2.0 software (Thermo Fisher Scientific) and manual inspection and interpretation of mass spectra.

Results

Body temperature

Compared to vehicle injection, 3 mg/kg CUMYL-PICA and 5F-CUMYL-PICA produced hypothermic effects in rats (Fig. 2). The mean rectal body temperature was significantly reduced following treatment with CUMYL-PICA at 15 and 30 min and 1, 2, and 4 h post-injection. Similarly, significant hypothermic effects were observed following 5F-CUMYL-PICA treatment at 15 and 30 min and 1, 2, and 4 h post-injection.

Liver microsome clearance

Clearance of CUMYL-PICA and 5F-CUMYL-PICA was rapid in rat and human liver microsome incubations (Fig. 3a–d; Table 1). However, both compounds were still detectible after 3 h incubations. Kinetic parameters were similar across all incubations except for CUMYL-PICA in human liver microsomes, which had a substantially longer half-life and correspondingly reduced extraction ratio.

Plasma kinetics

Following intraperitoneal administration of 3 mg/kg CUMYL-PICA or 5F-CUMYL-PICA, plasma concentrations of the parent compounds rose quickly, followed by gradual and incomplete elimination over the following 24 h (Fig. 3e, f). Table 1 contains parameters generated from non-compartmental analysis of the pharmacokinetic data. Overall, the pharmacokinetics of both compounds in rat plasma were similar, although the maximum concentration of CUMYL-PICA was greater and occurred earlier than that of 5F-CUMYL-PICA. CUMYL-PICA had a shorter half-life than 5F-CUMYL-PICA, and the apparent clearance (CL/F) values for both compounds were lower than clearance values predicted by microsome preparations.

CUMYL-PICA metabolism

Phase I metabolites

Phase I metabolism of CUMYL-PICA was extensive, with oxidation occurring at numerous sites (Figs. 4a, 5; Table 2). Parent CUMYL-PICA eluted at 8.94 min, and was confirmed by matching fragmentation and retention times with an analytical standard (Fig. 4a). The $[M+H]^+$ molecular ion of CUMYL-PICA was *m/z* 349.2258, and produced product ions at *m/z* 231.1472, 214.1220, and 188.1449, corresponding to fragmentation along the carboxamide linking group, and 119.0848 and 91.0542, corresponding to fragmentation of the α,α-dimethylbenzyl moiety and subsequent formation of a tropylium ion.

Six monohydroxylated metabolites (C21, C22, C24–C27) with *m/z* 365.2210 were identified in rat hepatocytes. Metabolites C26 and C27 were likely hydroxylated on the benzene ring of the α,α-dimethylbenzyl moiety, as they produced product ions at *m/z* 135.0791 and 107.0493, 15.99 Da higher than product ions at *m/z* 119.0848 and 91.0542 of the parent molecule, respectively. However, C26 and C27 were not observed in human hepatocyte incubations. Metabolites C21 and C22 produced an ion at *m/z* 161.0707, suggesting that hydroxylation did not occur on the indole moiety, and also produced a product ion at *m/z* 119.0848, excluding the α,α-dimethylbenzyl moiety, leaving the *N*-pentyl chain as the likely hydroxylation location. C24 and C25 lacked the ion at *m/z* 161; thus hydroxylation may have occurred on the indole moiety for these metabolites, although the expected product ions at *m/z* 160 and 177 (144 + 16 and 161 + 16) were not observed.

Although fragmentation was insufficient to localize each hydroxylation to the exact molecular site, corresponding data from 5F-CUMYL-PICA incubations were informative. A metabolite (F22) with retention time and fragmentation identical to that of C21 was also formed

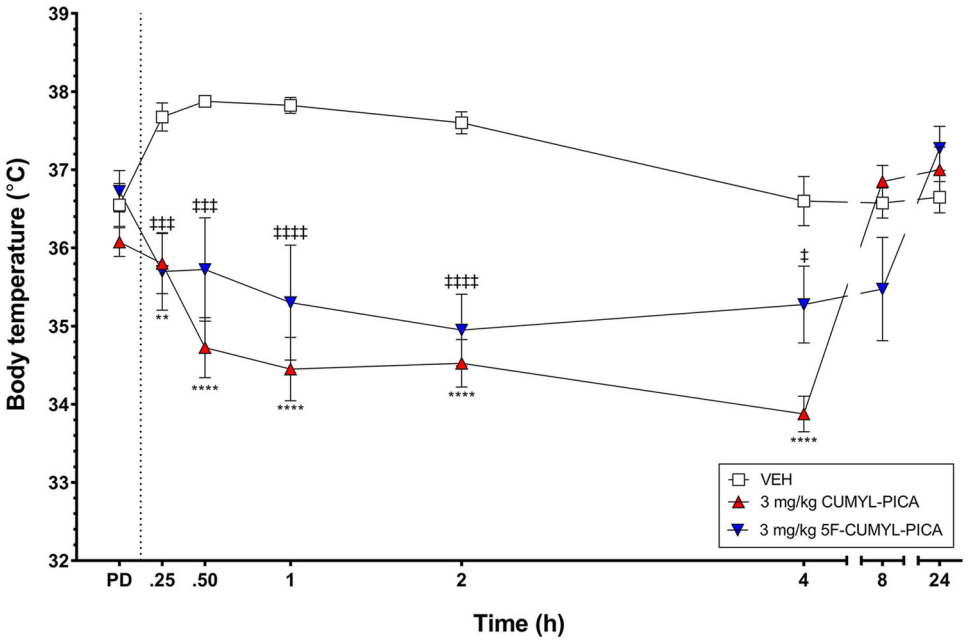

Fig. 2 Mean rectal body temperature of male rats following administration of vehicle solution or 3 mg/kg CUMYL-PICA or 5F-CUMYL-PICA ($n = 4$ per group). *Dashed line* denotes time of intraperitoneal (i.p.) injection. The *error bars* represent standard error of the mean (SEM). *$P < 0.05$, **$P < 0.01$, ***$P < 0.001$, ****$P < 0.0001$, comparing CUMYL-PICA to vehicle at each time point. ‡$P < 0.05$, ‡‡$P < 0.01$, ‡‡‡$P < 0.001$, ‡‡‡‡$P < 0.0001$, comparing 5F-CUMYL-PICA to vehicle at each time point. *PD* pre-dose, 15 min before injection; *VEH* vehicle

following hepatocyte incubation or rat dosing with 5F-CUMYL-PICA. Because this metabolite could only occur following oxidative defluorination of 5F-CUMYL-PICA, we conclude that metabolite C21 is hydroxylated at the terminal position of the *N*-pentyl chain. C21 was further oxidized to form a carboxylic acid metabolite C20 ($[M+H]^+$ *m/z* 379.2005). Product ions at *m/z* 200.1076 and 119.0848 exclude this transformation from the indole and α,α-dimethylbenzyl moieties, strongly suggesting formation of the carboxylic acid on the *N*-pentyl chain. Similar hydroxylation and carboxylation has been reported for AMB, 5F-AMB, JWH-018, AM-2201, RCS-4, UR-144, JWH-073, JWH-210, and others [15, 16, 21–24].

The monohydroxylated metabolites underwent further hydroxylation to form two dihydroxylated metabolites (C11 and C13) with *m/z* 381.2261 (Fig. 5; Table 2). Similar to metabolites C26 and C27, metabolite C11 was hydroxylated once on the α,α-dimethylbenzyl moiety based on product ion at *m/z* 135.0791, while the ion at *m/z* 144.0444 suggests that the other hydroxylation occurred on the *N*-pentyl chain. C13 produced product ions at *m/z* 263.1379 and 246.1144, 32 Da higher than CUMYL-PICA product ions at *m/z* 231.1472 and 214.1220, respectively, and also produced a product ion at *m/z* 119.0848, but not at *m/z* 135.0791, indicating that both hydroxylations occurred on the indole and/or *N*-pentyl moieties. In 5F-CUMYL-PICA preparations, we observed a metabolite (F15) with retention time and mass identical to those of C13; however product ions differed substantially, suggesting formation of a similar but non-identical dihydroxylated metabolite.

CUMYL-PICA was also carbonylated, forming metabolite C23 with $[M+H]^+$ *m/z* 363.2056. The product ions at *m/z* 245.1312 and 228.1023 were 13.98 Da larger than the corresponding CUMYL-PICA product ions at *m/z* 231.1472 and 214.1220 (i.e., +O–2H). Ions at *m/z* 119.0848 and 144.0444 indicate that this carbonylation did not occur on the α,α-dimethylbenzyl or indole moieties, respectively, while the product ion at *m/z* 85.0646 localized this transformation to the *N*-pentyl chain. Metabolite C28 had a molecular ion at *m/z* 347.2103, 2.0155 Da less than CUMYL-PICA, suggesting a dehydrogenation. Product ions at *m/z* 229.1315, 212.1048, 186.1290, and 119.0848 indicate that dehydrogenation occurred on the indole or *N*-pentyl moieties; however, this likely occurred on the *N*-pentyl chain, given the lack of suitable sites for dehydrogenation on the indole moiety, and in light of similar reports of dehydrogenation on the *N*-pentyl chain for other synthetic cannabinoids [15].

Additionally, CUMYL-PICA appears to undergo dealkylation of the *N*-pentyl chain, producing metabolite C18 with *m/z* 279.1978. The product ions at *m/z* 161.0707, 144.0444, 119.0848, 118.0642, and 91.0542 are consistent with this interpretation. Similar dealkylation occurred in some synthetic cannabinoids containing an *N*-pentyl or *N*-fluoropentyl chain [23, 25]. Four monohydroxylations of this metabolite were identified (*m/z* 295.1429). Two of these (C9 and C10) occurred on the indole moiety, evidenced by product ions at *m/z* 177.0669 and 160.0407, 16 Da higher than 161.0707 and 144.0444, respectively. The other two hydroxylations (C7 and C8) lacked these ions, and instead produced a product ion at *m/z* 135.0791 while retaining ions at *m/z* 161.0707 and 144.0444, strongly indicating that hydroxylation occurred on the α,α-dimethylbenzyl moiety.

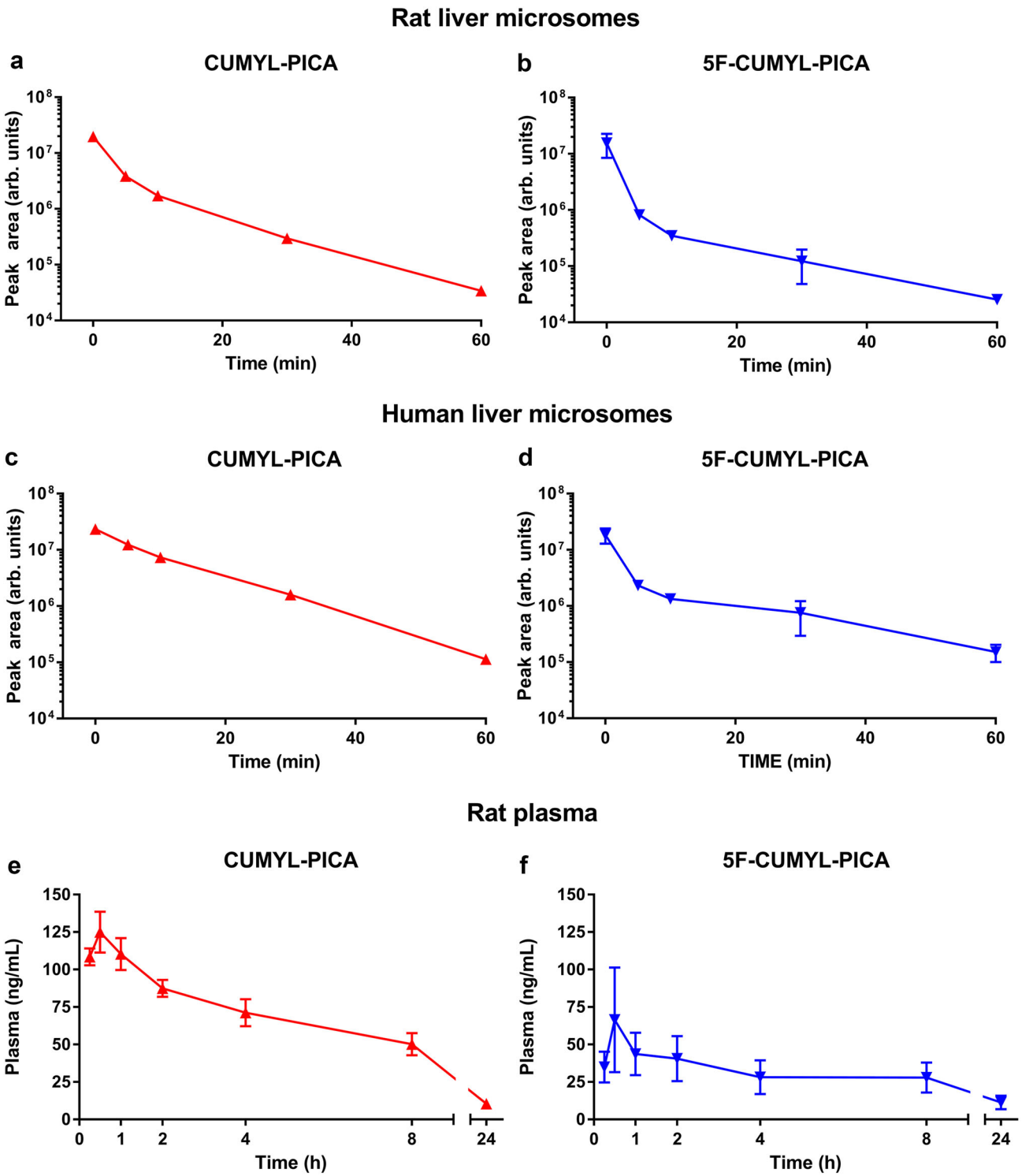

Fig. 3 Mean chromatographic peak areas of CUMYL-PICA and 5F-CUMYL-PICA following incubation with rat and human liver microsomes (panels **a**–**d**, $n = 3$), and mean plasma concentrations of CUMYL-PICA and 5F-CUMYL-PICA following a 3-mg/kg i.p. injection in male rats (panels **e** and **f**, $n = 4$). *Error bars* are SEM

Phase II metabolites

No direct phase II transformations of CUMYL-PICA were observed, but several phase I metabolites underwent glucuronidation. Five discrete peaks at *m/z* 541.2510 were identified in rat and human hepatocytes (C12, C14, C15, C17, and C19), 176 Da greater than monohydroxylated metabolites (*m/z* 365.2210), indicating glucuronidation. A

Table 1 Pharmacokinetic parameters of CUMYL-PICA and 5F-CUMYL-PICA incubated in rat and human liver microsomes in vitro and in rat plasma in vivo

Pharmacokinetic parameter	CUMYL-PICA	5F-CUMYL-PICA
Rat liver microsomes		
Half-life (min)	2.24	1.19
$CL_{int,micr}$ (mL/min/mg)	0.31	0.58
CL_{int} (mL/min/kg body wt.)	556.88	1048.24
CL_H (mL/min/kg body wt.)	50.22	52.44
ER	0.91	0.95
Human liver microsomes		
Half-life (min)	5.92	1.77
$CL_{int,micr}$ (mL/min/mg)	0.12	0.39
CL_{int} (mL/min/kg body wt.)	135.46	453.05
CL_H (mL/min/kg body wt.)	17.43	19.15
ER	0.87	0.96
Rat plasma		
Half-life (h)	7.26	12.00
CL/F (mL/min/kg body wt.)	43.31	147.88
C_{max} (ng/mL)	130.50	65.25
T_{max} (h)	0.50	0.50
AUC 0–24 h (h ng/mL)	1086.57	581.78
AUC 0–∞ (h ng/mL)	1214.85	843.28

AUC area under the curve, *CL/F* observed apparent clearance, CL_H estimated hepatic clearance, CL_{int} estimated intrinsic clearance, $CL_{int,\ micr}$ intrinsic microsome clearance, C_{max} mean maximum observed concentration, *ER* extraction ratio, T_{max} mean time of C_{max}

metabolite identical to C15 in mass, retention time, and product ions was observed in 5F-CUMYL-PICA incubations (F19), indicating that this metabolite is the glucuronide of C21. C19 was found following incubation with human hepatocytes, which likely excludes it as a glucuronide of the α,α-dimethylbenzyl hydroxylated metabolites (C26 and C27), because these metabolites were not found in human hepatocyte incubations (Table 2).

Dihydroxylated metabolites were glucuronidated to four identifiable glucuronides (C3–C5, C16). Mass spectral data were not sufficient to assign each glucuronide to a specific dihydroxylated metabolite. Interestingly, C16 was far more abundant and eluted much later than C3–C5 (Fig. 4a), indicating a substantially less polar structure. Carboxylic acid metabolite C20 formed glucuronide C6 (*m/z* 555.2334). Either C7 or C8 formed glucuronidated metabolite C1, which had a mass of *m/z* 471.1746 and product ions at *m/z* 161.0707, 144.0444, and 135.0791. Similarly, C9 or C10 was glucuronidated to C2 ($[M+H]^+$ *m/z* 471.1746, product ions at *m/z* 177.0669, 160.0407, and 119.0848). No sulfation or other phase II transformations were observed.

5F-CUMYL-PICA metabolism

Phase I metabolites

Similar to CUMYL-PICA, 5F-CUMYL-PICA was extensively oxidized and glucuronidated (Fig. 6; Table 3). The $[M+H]^+$ molecular ion was *m/z* 367.2161 for the unaltered compound, and major product ions were *m/z* 249.1417, 232.1116, and 206.1317, all 17.99 Da higher than corresponding CUMYL-PICA ions (i.e., +F−H), in addition to identical ions at *m/z* 119.0848 and 91.0542. Compound identity was also confirmed by matching retention time and fragmentation to the reference standard (retention time 8.11 min; Fig. 4b).

Six monohydroxylations of 5F-CUMYL-PICA were identified (F23–F28, *m/z* 383.2103, 15.99 Da larger than parent). Metabolites F23–F25 and F27 produced a product ion at *m/z* 119.0848, suggesting hydroxylation on the indole or *N*-fluoropentyl moiety, while metabolites F26 and F28 produced an ion at *m/z* 135.0791, indicating hydroxylation on the α,α-dimethylbenzyl moiety. Unfortunately, metabolites F23–F25 and F27 did not produce product ions that might be used to distinguish between indole or *N*-fluoropentyl chain oxidations (e.g., 144 vs 160, or 161 vs 177). However, we suggest that 5F-CUMYL-PICA hydroxylation likely proceeds in a manner similar to CUMYL-PICA, and that these metabolites are likely 5-fluoropentyl analogues of CUMYL-PICA metabolites C22, C24, and C25.

Dihydroxylated metabolites F14 and F17 were also detected. F14 produced a product ion at *m/z* 135.0791 suggesting that one hydroxylation occurred on the α,α-dimethylbenzyl moiety, while ions at *m/z* 265.1363 and 248.1018 indicate that the other hydroxylation occurred on the indole or *N*-fluoropentyl portion of the molecule. F17 produced ion at *m/z* 119.0848 instead of *m/z* 135.0791, suggesting both hydroxylations occurred on the indole or *N*-fluoropentyl portion of the molecule. This interpretation is supported by the presence of ions at *m/z* 281.1266 and 264.1018 (15.99 Da higher than ions at *m/z* 265.1363 and 248.1107, respectively).

Oxidative defluorination was a predominant metabolic pathway, forming metabolite F22 at *m/z* 365.2210 and product ions at *m/z* 247.1448, 230.1149, 204.1378, and 119.0848, identical to CUMYL-PICA metabolite C21. Similar dehalogenation has been reported as a major metabolic pathway for AM-2201, 5F-AMB, XLR-11, and AM-694 [15, 22, 26]. Additional hydroxylation of F22 produced dihydroxylated metabolite F15 ($[M+H]^+$ *m/z* 381.2169), which produced ions at *m/z* 263.1379, 246.1144, 202.1207, and 119.0848, indicating that the second hydroxylation occurred on the pentyl chain or indole moiety. Oxidation of F22 formed carboxylic acid

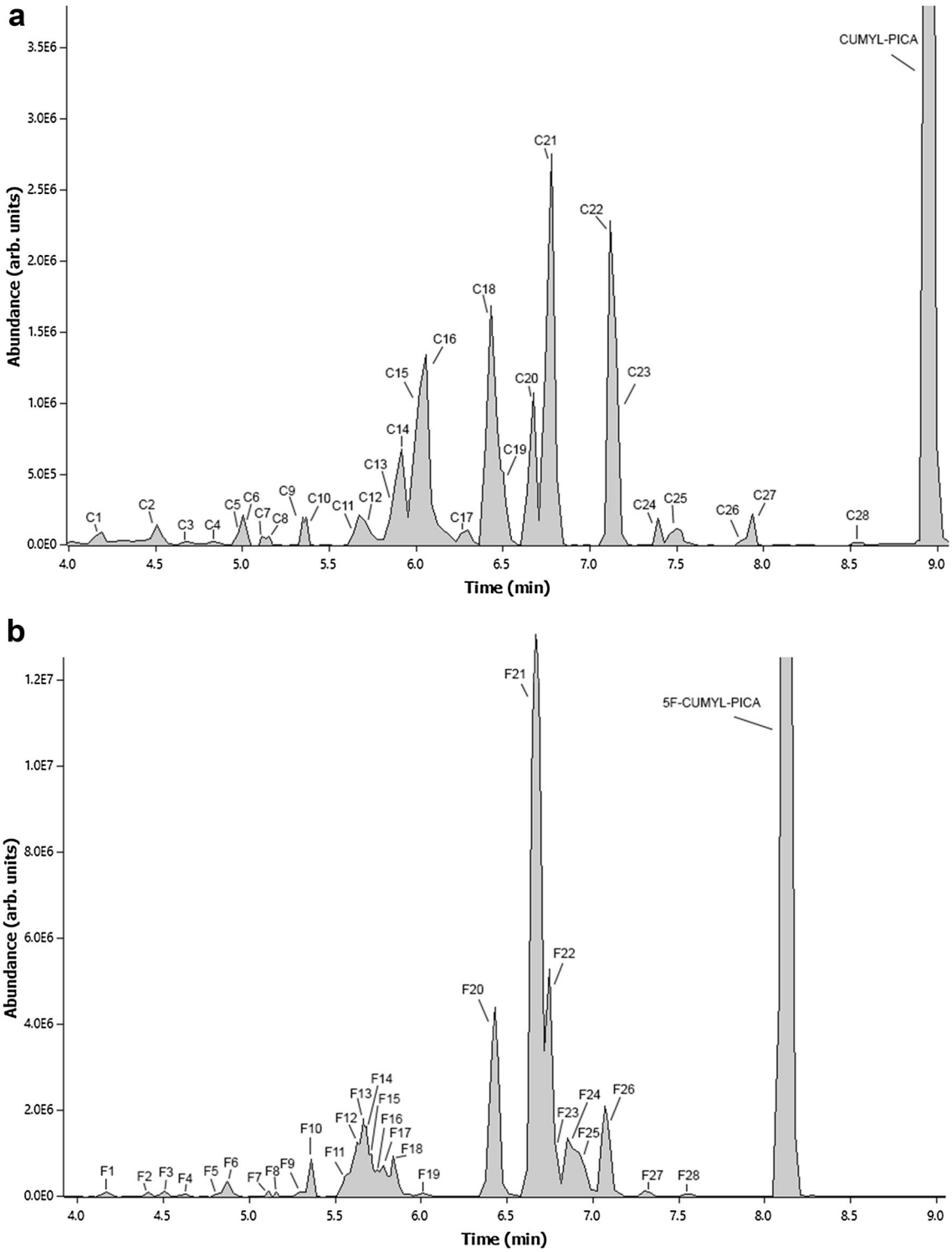

Fig. 4 Combined extracted ion chromatograms of **a** CUMYL-PICA and **b** 5F-CUMYL-PICA metabolites after 3-h incubation with rat hepatocytes, obtained by liquid chromatography–single-stage mass spectrometry

metabolite F21, identical to CUMYL-PICA metabolite C20. F21 was then hydroxylated, forming metabolites F11 and F13 ($[M+H]^+$ *m/z* 395.1937). F11 produced product ion at *m/z* 135.0791, indicating hydroxylation on the α,α-dimethylbenzyl moiety, and ion at *m/z* 200.1076 further localized this modification to the benzene ring. F13 produced ions at *m/z* 277.1163, 260.0936, 216.1009, and 119.0848, suggesting hydroxylation of the indole

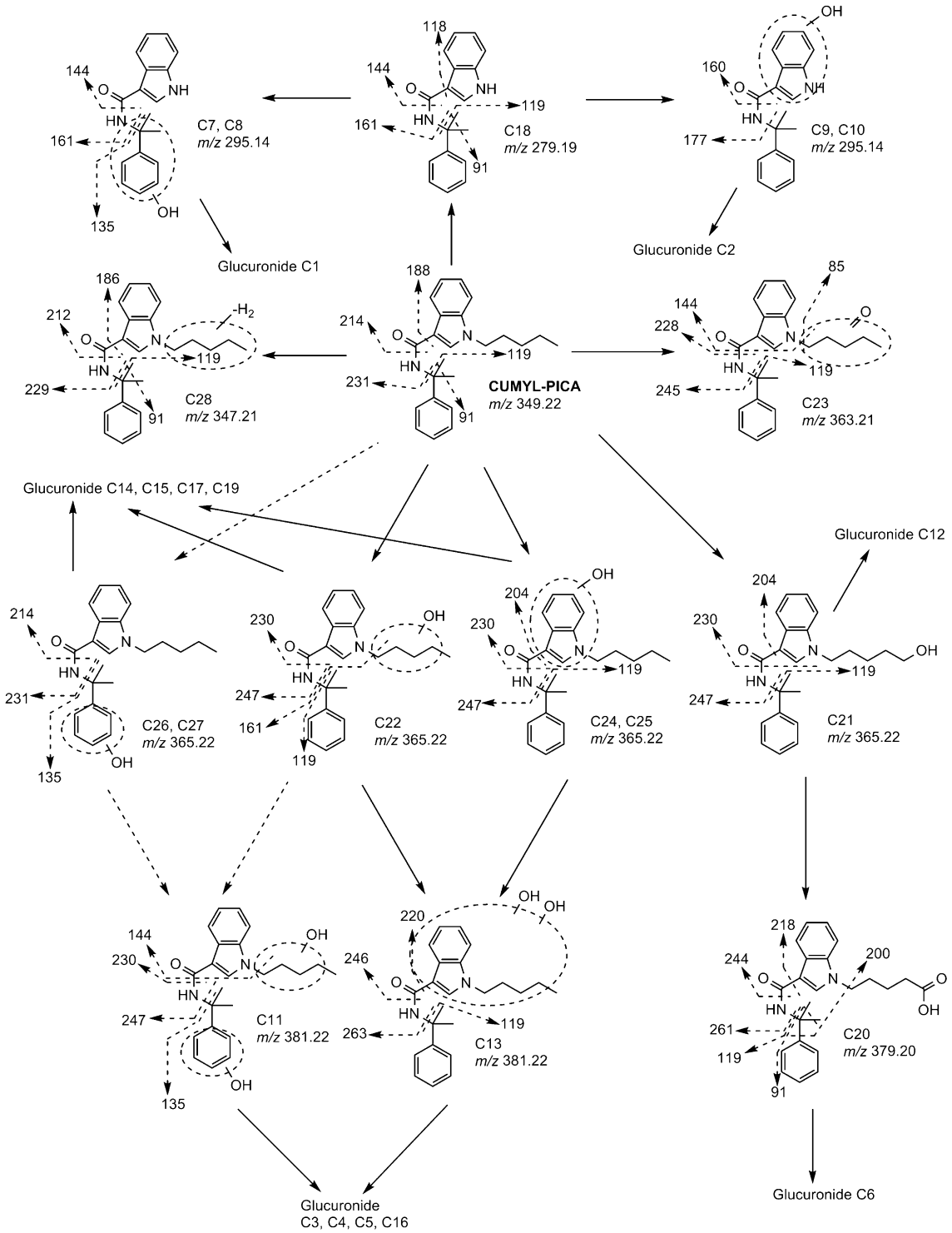

Fig. 5 Proposed CUMYL-PICA metabolic pathways in rats and humans. *Dashed arrows* between compounds denote formation of metabolites that were not observed in human hepatocyte incubations. Unlocalized transformations are shown as Markush structures

moiety. Interestingly, these hydroxylation reactions were not detected in CUMYL-PICA incubations. Oxidative defluorination may occur more readily than terminal hydroxylation of the *N*-pentyl chain, thereby increasing concentrations of subsequent metabolites. This is supported by our chromatographic data that show a larger extracted ion peak (*m/z* 365.2) for F22 compared to C21 (Fig. 4).

Table 2 CUMYL-PICA metabolites following incubation with rat and human hepatocytes, and their presence in rat plasma and urine following a 3-mg/kg intraperitoneal (i.p.) injection

Metabolite	RT (min)	Transformation	Molecular ion $[M+H]^+$ (*m/z*)	Major product ion(s) (*m/z*)	Rat hepatocyte	Human hepatocyte	Rat plasma	Rat urine
C1	4.15	*N*-Pentyl dealkylation + hydroxylation (α,α-dimethylbenzyl) + glucuronidation	471.17	177, 161, 135	✔			✔
C2	4.51	*N*-Pentyl dealkylation + hydroxylation (indole) + glucuronidation	471.17	177, 119	✔	✔		✔
C3	4.68	Dihydroxylation + glucuronidation	557.24	381, 263	✔	✔		
C4	4.83	Dihydroxylation + glucuronidation	557.24	381, 263	✔	✔		
C5	4.95	Dihydroxylation + glucuronidation	557.24	381, 263	✔	✔		
C6	5.01	Carboxylation + glucuronidation	555.23	379	✔	✔		✔
C7	5.11	*N*-Pentyl dealkylation + hydroxylation (α,α-dimethylbenzyl)	295.14	161, 144, 135	✔	✔	✔	
C8	5.17	*N*-Pentyl dealkylation + hydroxylation (α,α-dimethylbenzyl)	295.14	161, 144, 135	✔		✔	
C9	5.30	*N*-Pentyl dealkylation + hydroxylation (indole)	295.14	177, 160	✔	✔		
C10	5.34	*N*-Pentyl dealkylation + hydroxylation (indole)	295.14	177, 160	✔	✔	✔	
C11	5.65	Dihydroxylation (α,α-dimethylbenzyl, *N*-pentyl)	381.22	247, 230, 144, 135	✔		✔	
C12	5.78	Hydroxylation + glucuronidation	541.25	365, 230	✔	✔		
C13	5.87	Dihydroxylation (*N*-pentyl, indole)	381.22	263, 246, 220, 119	✔	✔	✔	
C14	5.92	Hydroxylation + glucuronidation	541.25	365, 230	✔			
C15	6.02	Hydroxylation (*N*-pentyl, terminal) + glucuronidation	541.25	423, 247, 230, 204, 119	✔	✔		✔
C16	6.12	Dihydroxylation + glucuronidation	557.24	381, 263	✔	✔		
C17	6.30	Hydroxylation + glucuronidation	541.25	365, 230	✔			
C18	6.41	*N*-Pentyl dealkylation	279.19	161, 144, 119, 118, 91	✔	✔		
C19	6.50	Hydroxylation + glucuronidation	541.25	365, 230	✔	✔	✔	
C20	6.68	Carboxylation	379.20	261, 244, 218, 200, 119, 91	✔	✔	✔	
C21	6.76	Hydroxylation (*N*-pentyl, terminal)	365.22	247, 230, 204, 119	✔	✔	✔	✔
C22	7.11	Hydroxylation (*N*-pentyl)	365.22	247, 230, 161, 119	✔	✔	✔	
C23	7.13	Carbonylation (*N*-pentyl)	363.21	245, 228, 144, 119, 85	✔	✔	✔	
C24	7.37	Hydroxylation (indole)	365.22	247, 230, 204, 119	✔	✔	✔	✔
C25	7.46	Hydroxylation (indole)	365.22	247, 230, 204, 119	✔	✔	✔	
C26	7.80	Hydroxylation (benzene ring)	365.22	231, 214, 135	✔			
C27	7.86	Hydroxylation (benzene ring)	365.22	231, 214, 135	✔		✔	
C28	8.52	Dehydrogenation (*N*-pentyl)	347.21	229, 212, 186, 119, 91	✔	✔	✔	
CUMYL-PICA	8.94	Parent compound	349.22	231, 214, 188, 119, 91	✔	✔	✔	

Ticks denote detection of compounds in a given matrix

RT retention time

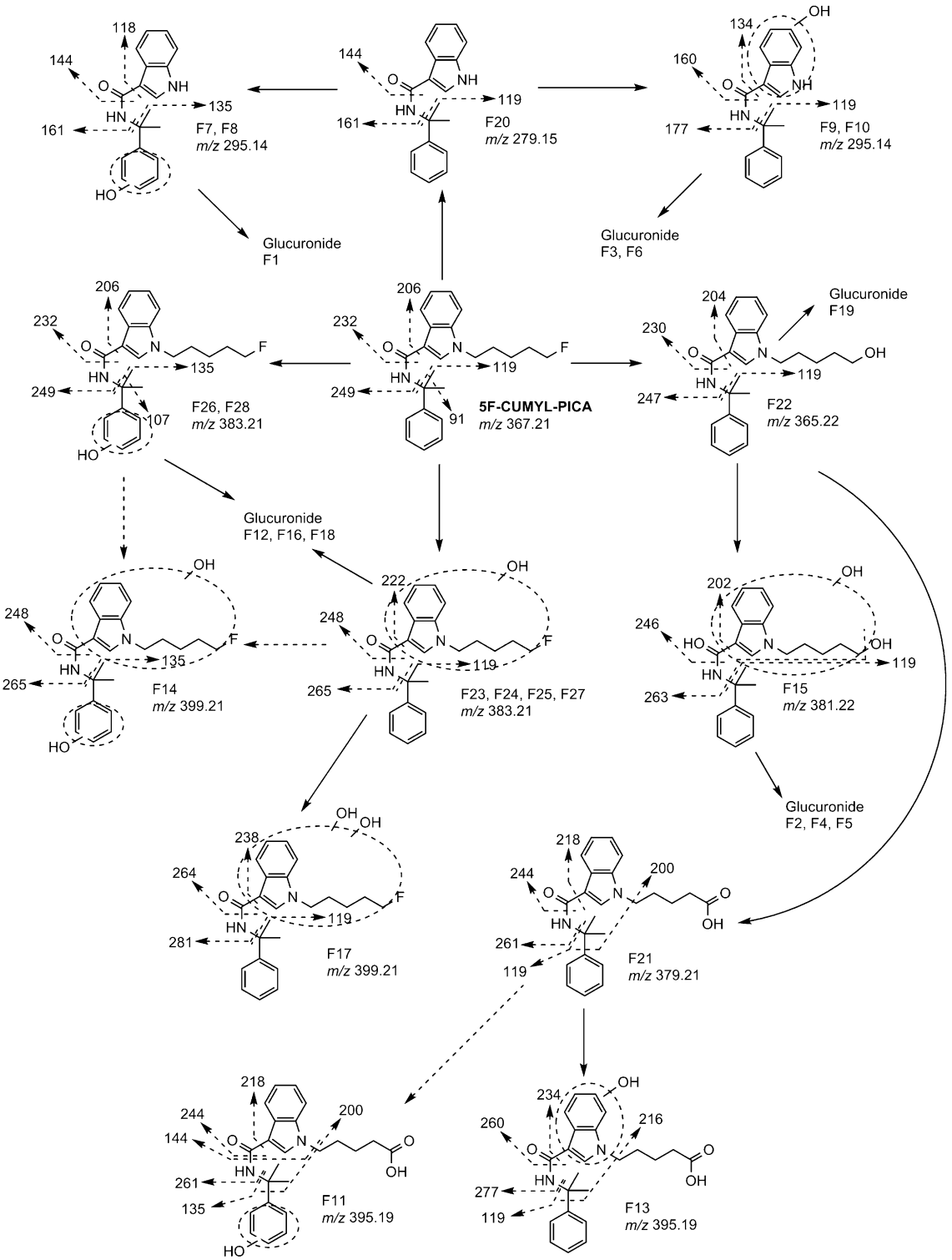

Fig. 6 Proposed 5F-CUMYL-PICA metabolic pathways in rats and humans. *Dashed arrows* between compounds denote formation of metabolites that were not observed in human hepatocyte incubations. Unlocalized transformations are shown as Markush structures

Similar to CUMYL-PICA, the *N*-fluoropentyl chain of 5F-CUMYL-PICA was eliminated, leaving metabolite F20, identical in retention time and fragmentation to CUMYL-PICA metabolite C18. As was the case for C18, F20 was further oxidized on the α,α-dimethylbenzyl moiety (F7 and F8, product ions at *m/z* 161.0707, 144.0444, 135.0791) or indole moiety (F9 and F10, product ions at *m/z* 177.0669, 160.0376, 119.0848).

Table 3 5F-CUMYL-PICA metabolites following incubation with rat and human hepatocytes, and in rat plasma and urine following a 3 mg/kg i.p. injection

Metabolite	RT (min)	Transformation	Molecular ion $[M+H]^+$ (*m/z*)	Major product ions (*m/z*)	Rat hepatocyte	Human hepatocyte	Rat plasma	Rat urine
F1	4.15	Fluoropentyl dealkylation + hydroxylation (α,α-dimethylbenzyl) + glucuronidation	471.17	177, 161, 135	✔			✔
F2	4.44	Oxidative defluorination + hydroxylation + glucuronidation	557.24	381, 263	✔			
F3	4.51	Fluoropentyl dealkylation + hydroxylation (indole) + glucuronidation	471.17	177, 119	✔	✔	✔	✔
F4	4.65	Oxidative defluorination + hydroxylation + glucuronidation	557.24	381, 263	✔	✔	✔	
F5	4.80	Oxidative defluorination + hydroxylation + glucuronidation	557.24	381, 263	✔	✔		
F6	4.87	Fluoropentyl dealkylation + hydroxylation (indole) + glucuronidation	471.17	177, 119	✔	✔		✔
F7	5.11	Fluoropentyl dealkylation + hydroxylation (α,α-dimethylbenzyl)	295.14	161, 144, 135, 118	✔	✔	✔	
F8	5.17	Fluoropentyl dealkylation + hydroxylation (α,α-dimethylbenzyl)	295.14	161, 144, 135, 118	✔	✔	✔	
F9	5.30	Fluoropentyl dealkylation + hydroxylation (indole)	295.14	177, 160, 134, 119	✔	✔	✔	
F10	5.34	Fluoropentyl dealkylation + hydroxylation (indole)	295.14	177, 160, 134, 119	✔	✔	✔	
F11	5.58	Oxidative defluorination + carboxylation + hydroxylation (α,α-dimethylbenzyl)	395.19	261, 244, 218, 200, 144, 135	✔		✔	
F12	5.61	Hydroxylation + glucuronidation	559.24	382, 248	✔			
F13	5.64	Oxidative defluorination + carboxylation + hydroxylation (indole)	395.19	277, 260, 234, 216, 119	✔	✔	✔	
F14	5.66	Dihydroxylation (α,α-dimethylbenzyl, indole/fluoropentyl)	399.21	265, 248, 135	✔		✔	
F15	5.68	Oxidative defluorination + oxidation	381.22	263, 246, 202, 119	✔	✔		
F16	5.70	Hydroxylation + glucuronidation	559.24	382, 248	✔	✔	✔	
F17	5.72	Dihydroxylation (indole/fluoropentyl)	399.21	281, 264, 238, 119	✔	✔	✔	
F18	5.78	Hydroxylation + glucuronidation	559.24	382, 248	✔	✔	✔	✔
F19	6.01	Oxidative defluorination + glucuronidation	541.25	247, 230, 204, 186, 119	✔			
F20	6.42	Fluoropentyl dealkylation	279.15	161, 144, 119	✔	✔	✔	
F21	6.68	Oxidative defluorination + carboxylation	379.21	261, 244, 218, 200, 119	✔	✔	✔	
F22	6.74	Oxidative defluorination	365.22	247, 230, 204, 119	✔	✔	✔	
F23	6.79	Hydroxylation (indole, fluoropentyl)	383.21	265, 248, 222, 119	✔	✔	✔	
F24	6.85	Hydroxylation (indole, fluoropentyl)	383.21	265, 248, 222, 119	✔	✔	✔	
F25	6.92	Hydroxylation (indole, fluoropentyl)	383.21	265, 248, 222, 119	✔		✔	
F26	7.03	Hydroxylation (benzene)	383.21	249, 232, 206, 135, 107	✔	✔	✔	
F27	7.31	Hydroxylation (indole, fluoropentyl)	383.21	265, 248, 222, 119	✔		✔	
F28	7.55	Hydroxylation (benzene)	383.21	249, 232, 206, 135, 107	✔			
5F-CUMYL-PICA	8.11	Parent compound	367.21	249, 232, 206, 119, 91	✔	✔	✔	

Ticks denote detection of compounds in a given matrix

Phase II metabolites

As was the case for CUMYL-PICA, 5F-CUMYL-PICA did not undergo direct phase II metabolism. Monohydroxylated metabolites formed three glucuronides of mass 559.2445 (F12, F16, and F18). Like monohydroxylated CUMYL-PICA glucuronides, mass spectra were not sufficient to localize each glucuronidation to a specific monohydroxylated metabolite.

Oxidatively defluorinated metabolite F22 was glucuronidated to F19, which was identical in retention time and fragmentation to CUMYL-PICA metabolite C12. F15, the hydroxylated metabolite of F22, was also glucuronidated. Interestingly, three distinct glucuronidations were identified (F2, F4, and F5). It is likely that glucuronidation occurred on either hydroxyl group of F15, which accounts for two glucuronides, but the presence of a third glucuronidated compound suggests that an additional dihydroxylated metabolite may have been formed but not detected.

F9 and F10 were glucuronidated to F3 and F6 ($[M+H]^+$ *m/z* 471.1746, product ions at *m/z* 177.0669, 160.0407, and 119.0848), while either F7 or F8 was glucuronidated to F1 ($[M+H]^+$ 471.1746, product ions at *m/z* 161.0707, 144.0444, and 135.0791). No sulfation or other phase II transformations were observed.

Discussion

This study examined the metabolism and clearance of synthetic cannabinoids CUMYL-PICA and 5F-CUMYL-PICA in rat and human liver microsomes and hepatocytes (in vitro), and in whole animals following administration of each compound in adult male rats. Both compounds produced moderate hypothermic effects at an intraperitoneal dose of 3 mg/kg. While rapid clearance for both compounds was predicted by in vitro data, actual elimination in vivo occurred slowly (Fig. 3). Both compounds were extensively metabolized via oxidative transformations and subsequent glucuronidation, and produced several identical metabolites.

CUMYL-PICA and 5F-CUMYL-PICA produced hypothermic effects of similar magnitude across a 4–8-h period (Fig. 2). For the most part, the magnitude of hypothermia was mirrored by blood drug concentration, although there was some delay between peak hypothermia and peak blood concentration. Rats dosed with CUMYL-PICA also returned to baseline body temperature more rapidly than might be expected from blood concentration. This could be the result of homeostatic mechanisms including rapid receptor internalization or down-regulation. Analogous hypothermic effects in rodents have been observed following administration of a wide variety of number of CB_1 agonists, including other synthetic cannabinoids [1, 2, 27–29] and phytocannabinoids [30]. These effects are blocked by the CB_1 antagonist rimonabant (SR141716), indicating a CB_1-dependent mechanism [2, 31]. Although we did not block hypothermia with rimonabant in this study, it is likely that CUMYL-PICA and 5F-CUMYL-PICA produce hypothermia via CB_1 given their structural similarity to several synthetic cannabinoids assessed in previous reports.

Although rapid clearance of CUMYL-PICA and 5F-CUMYL-PICA was observed in microsomal incubations, rat plasma half-lives were 7 and 12 h, respectively, and both untransformed compounds were detectible in plasma at 24 h post-dosing (Fig. 3; Table 1). In addition, apparent in vivo clearance was substantially slower than clearance values predicted by microsomal incubations. Several factors may account for this discrepancy; lipophilicity seems to be the most likely contributor. These compounds, including Δ^9-tetrahydrocannabinol (Δ^9-THC), are largely non-polar and dissolve poorly in aqueous solutions. In rats and humans, Δ^9-THC is sequestrated into adipose tissue and appears to passively and slowly diffuse back into blood during satiety [32, 33], or more rapidly during periods of food deprivation [34]. In a case of fatal poisoning involving synthetic cannabinoids AB-CHMINACA and 5F-AMB, unaltered parent compounds were found at higher levels in adipose tissue than in blood [35]. Thus it is plausible that similar sequestration of CUMYL-PICA and 5F-CUMYL-PICA in adipose tissue, followed by slow passive diffusion back into blood, could be at least partly responsible for the long half-lives of these compounds in vivo. Analysis of adipose tissue following synthetic cannabinoid administration may prove fruitful in future studies. It should also be noted that our in vitro calculations ignored protein binding, because it is presently uncharacterized for CUMYL-PICA and 5F-CUMYL-PICA. Regardless of the mechanisms, the rapid clearance of synthetic cannabinoids in microsomal incubations observed in this and similar studies should be interpreted with caution in light of rodent data and human case studies that point to long elimination periods in vivo.

A total of 28 metabolites of CUMYL-PICA and 28 metabolites of 5F-CUMYL-PICA were identified in hepatocyte preparations. However, some metabolites produced small peaks (Fig. 4), and subsets of 18 and 22 metabolites were detectable in rat plasma or urine for CUMYL-PICA and 5F-CUMYL-PICA, respectively (Tables 2, 3). CUMYL-PICA and 5F-CUMYL-PICA were generally metabolized similarly by rat and human hepatocytes, although a notable exception was that hydroxylation of the α,α-dimethylbenzyl moiety was rarely observed using human hepatocytes. Unsurprisingly, a greater number of phase I metabolites were detected in plasma than in urine, and most metabolites detected in urine were glucuronides. For urinalysis, glucuronide hydrolysis is recommended in

order to increase urinary metabolite concentrations to aid detection and identification. Extensive glucuronidation appears to be common in the metabolism of other synthetic cannabinoids [14, 15, 36] and phytocannabinoids [37, 38].

The terminally hydroxylated metabolite of CUMYL-PICA was abundant (as measured semi-quantitatively by peak area; Fig. 4), but it was identical to the oxidatively defluorinated metabolite of 5F-CUMYL-PICA. Similarly, the carboxylated metabolite of 5F-CUMYL-PICA was abundant but identical to the corresponding CUMYL-PICA metabolite. Consequently, CUMYL-PICA and 5F-CUMYL-PICA cannot be distinguished from each other using either of their most abundant metabolites. Additionally, elimination of the *N*-pentyl or 5-fluoropentyl chains of CUMYL-PICA and 5F-CUMYL-PICA, respectively, formed identical metabolites. Similar metabolic convergence has been observed with other pairs of structurally related compounds, including AMB and 5F-AMB, JWH-018 and AM-2201, and UR-144 and XLR-11 [15, 23].

Considering these data, analytical targets for forensic purposes must be selected with care. Long elimination periods in vivo suggest that screening for parent compounds in blood may be sufficient in cases of acute exposure. For less recent exposure, monohydroxylated metabolites are potentially useful analytical targets in these matrices, because they (or their glucuronides) were observed at levels well above detection thresholds. For CUMYL-PICA, a reasonable strategy would be to target monohydroxylations occurring on the indole moiety (considering that α,α-dimethylbenzyl hydroxylation was not observed in human hepatocyte preparations). Such hydroxylation was difficult to distinguish from the terminally hydroxylated metabolite, but the presence of more than one monohydroxylated metabolite at *m/z* 365 would be selective for CUMYL-PICA. For 5F-CUMYL-PICA, monohydroxylated metabolites retaining the terminal fluorine may be useful analytical targets.

Conclusions

CUMYL-PICA and 5F-CUMYL-PICA produced moderate hypothermic effects in male rats, and both compounds were metabolized primarily via oxidative transformations followed by glucuronidation in both rat and human models. In vivo clearance of CUMYL-PICA and 5F-CUMYL-PICA was substantially longer than predicted by in vitro incubations, possibly due to the high lipophilicity of these compounds or blood-protein binding. As is the case for other structurally related pairs of synthetic cannabinoids, formation of identical metabolites necessitates careful selection of analytical targets in order to differentiate between CUMYL-PICA and 5F-CUMYL-PICA.

Acknowledgements RCK was supported by an Australian Postgraduate Award. ISM was supported by a National Health and Medical Research Council fellowship. This work was supported by research grant funding to BFT from the National Institute on Drug Abuse (1R01DA-040460), to JLW from the National Institutes of Health (DA-03672), internal research and development funds provided by the Research Triangle Institute, NC, USA, and from the Lambert Initiative for Cannabinoid Therapeutics, NSW, Australia.

Compliance with ethical standards

Conflict of interest The authors have no conflict of interest to declare.

Ethical approval All applicable international, national, and/or institutional guidelines for the care and use of animals were followed. All procedures performed in studies involving animals were in accordance with the ethical standards of the institution at which the studies were conducted.

References

1. Wiley JL, Marusich JA, Lefever TW, Antonazzo KR, Wallgren MT, Cortes RA, Patel PR, Grabenauer M, Moore KN, Thomas BF (2015) AB-CHMINACA, AB-PINACA, and FUBIMINA: affinity and potency of novel synthetic cannabinoids in producing Δ^9-tetrahydrocannabinol-like effects in mice. J Pharmacol Exp Ther 354:328–339
2. Banister SD, Moir M, Stuart J, Kevin RC, Wood KE, Longworth M, Wilkinson SM, Beinat C, Buchanan AS, Glass M, Connor M, McGregor IS, Kassiou M (2015) The pharmacology of indole and indazole synthetic cannabinoid designer drugs AB-FUBINACA, ADB-FUBINACA, AB-PINACA, ADB-PINACA, 5F-AB-PINACA, 5F-ADB-PINACA, ADBICA and 5F-ADBICA. ACS Chem Neurosci 6:1546–1559
3. Wiebelhaus JM, Poklis JL, Poklis A, Vann RE, Lichtman AH, Wise LE (2012) Inhalation exposure to smoke from synthetic "marijuana" produces potent cannabimimetic effects in mice. Drug Alcohol Depend 126:316–323
4. Winstock AR, Barratt MJ (2013) Synthetic cannabis: a comparison of patterns of use and effect profile with natural cannabis in a large global sample. Drug Alcohol Depend 131:106–111
5. Kevin RC, Wood KE, Stuart J, Mitchell AJ, Moir M, Banister SD, Kassiou M, McGregor IS (2017) Acute and residual effects in adolescent rats resulting from exposure to the novel synthetic cannabinoids AB-PINACA and AB-FUBINACA. J Psychopharmacol. doi:10.1177/0269881116684336
6. Trecki J, Gerona RR, Schwartz MD (2015) Synthetic cannabinoid-related illnesses and deaths. N Engl J Med 373:103–107
7. Schwartz MD, Trecki J, Edison LA, Steck AR, Arnold JK, Gerona RR (2015) A common source outbreak of severe delirium associated with exposure to the novel synthetic cannabinoid ADB-PINACA. J Emerg Med 48:573–580
8. Khan M, Pace L, Truong A, Gordon M, Moukaddam N (2016) Catatonia secondary to synthetic cannabinoid use in two patients with no previous psychosis. Am J Addict 25:25–27
9. Louh IK, Freeman WD (2014) A 'spicy' encephalopathy: synthetic cannabinoids as cause of encephalopathy and seizure. Crit Care 18:553. doi:10.1186/s13054-014-0553-6
10. EMCDDA (2015) European drug report 2015. http://www.emcdda.europa.eu/attachements.cfm/att_239505_EN_TDAT15001ENN.pdf. Accessed 4 Oct 2015

11. EMCDDA (2014) Annual report on the implementation of the council decision 2005/387/JHA. http://www.emcdda.europa.eu/system/files/publications/1018/TDAN15001ENN.pdf. Accessed 5 Mar 2015
12. Hess C, Murach J, Krueger L, Scharrenbroch L, Unger M, Madea B, Sydow K (2016) Simultaneous detection of 93 synthetic cannabinoids by liquid chromatography-tandem mass spectrometry and retrospective application to real forensic samples. Drug Test Anal. doi:10.1002/dta.2030
13. Vikingsson S, Gréen H, Brinkhagen L, Mukhtar S, Josefsson M (2015) Identification of AB-FUBINACA metabolites in authentic urine samples suitable as urinary markers of drug intake using liquid chromatography quadrupole tandem time of flight mass spectrometry. Drug Test Anal 8:950–956
14. Thomsen R, Nielsen LM, Holm NB, Rasmussen HB, Linnet K, the IC (2015) Synthetic cannabimimetic agents metabolized by carboxylesterases. Drug Test Anal 7:565–576
15. Andersson M, Diao X, Wohlfarth A, Scheidweiler KB, Huestis MA (2016) Metabolic profiling of new synthetic cannabinoids AMB and 5F-AMB by human hepatocyte and liver microsome incubations and high-resolution mass spectrometry. Rapid Commun Mass Spectrom 30:1067–1078
16. Brents LK, Reichard EE, Zimmerman SM, Moran JH, Fantegrossi WE, Prather PL (2011) Phase I hydroxylated metabolites of the K2 synthetic cannabinoid JWH-018 retain in vitro and in vivo cannabinoid 1 receptor affinity and activity. PLoS One 6:e21917. doi:10.1371/journal.pone.0021917
17. Seely KA, Brents LK, Radominska-Pandya A, Endres GW, Keyes GS, Moran JH, Prather PL (2012) A major glucuronidated metabolite of JWH-018 is a neutral antagonist at CB1 receptors. Chem Res Toxicol 25:825–827
18. Davies B, Morris T (1993) Physiological parameters in laboratory animals and humans. Pharm Res 10:1093–1095
19. McNaney CA, Drexler DM, Hnatyshyn SY, Zvyaga TA, Knipe JO, Belcastro JV, Sanders M (2008) An automated liquid chromatography-mass spectrometry process to determine metabolic stability half-life and intrinsic clearance of drug candidates by substrate depletion. Assay Drug Dev Technol 6:121–129
20. Baranczewski P, Stanczak A, Sundberg K, Svensson R, Wallin A, Jansson J, Garberg P, Postlind H (2006) Introduction to in vitro estimation of metabolic stability and drug interactions of new chemical entities in drug discovery and development. Pharmacol Rep 58:453–472
21. Rajasekaran M, Brents LK, Franks LN, Moran JH, Prather PL (2013) Human metabolites of synthetic cannabinoids JWH-018 and JWH-073 bind with high affinity and act as potent agonists at cannabinoid type-2 receptors. Toxicol Appl Pharmacol 269:100–108
22. Knittel JL, Holler JM, Chmiel JD, Vorce SP, Magluilo J, Levine B, Ramos G, Bosy TZ (2016) Analysis of parent synthetic cannabinoids in blood and urinary metabolites by liquid chromatography tandem mass spectrometry. J Anal Toxicol 40:173–186
23. Sobolevsky T, Prasolov I, Rodchenkov G (2012) Detection of urinary metabolites of AM-2201 and UR-144, two novel synthetic cannabinoids. Drug Test Anal 4:745–753
24. Hutter M, Broecker S, Kneisel S, Auwärter V (2012) Identification of the major urinary metabolites in man of seven synthetic cannabinoids of the aminoalkylindole type present as adulterants in 'herbal mixtures' using LC-MS/MS techniques. J Mass Spectrom 47:54–65
25. Sobolevsky T, Prasolov I, Rodchenkov G (2010) Detection of JWH-018 metabolites in smoking mixture post-administration urine. Forensic Sci Int 200:141–147
26. Grigoryev A, Kavanagh P, Melnik A (2013) The detection of the urinary metabolites of 1-[(5-fluoropentyl)-1*H*-indol-3-yl]-(2-iodophenyl)methanone (AM-694), a high affinity cannabimimetic, by gas chromatography–mass spectrometry. Drug Test Anal 5:110–115
27. Banister SD, Stuart J, Kevin RC, Edington A, Longworth M, Wilkinson SM, Beinat C, Buchanan AS, Hibbs DE, Glass M, Connor M, McGregor IS, Kassiou M (2015) The effects of bioisosteric fluorine in synthetic cannabinoid designer drugs JWH-018, AM-2201, UR-144, XLR-11, PB-22, 5F-PB-22, APICA, and STS-135. ACS Chem Neurosci 6:1445–1458
28. Wiley JL, Marusich JA, Lefever TW, Grabenauer M, Moore KN, Thomas BF (2013) Cannabinoids in disguise: Δ^9-tetrahydrocannabinol-like effects of tetramethylcyclopropyl ketone indoles. Neuropharmacology 75:145–154
29. Wiley JL, Marusich JA, Martin BR, Huffman JW (2012) 1-Pentyl-3-phenylacetylindoles and JWH-018 share *in vivo* cannabinoid profiles in mice. Drug Alcohol Depend 123:148–153
30. Banister SD, Wilkinson SM, Longworth M, Stuart J, Apetz N, English K, Brooker L, Goebel C, Hibbs DE, Glass M, Connor M, McGregor IS, Kassiou M (2013) The synthesis and pharmacological evaluation of adamantane-derived indoles: cannabimimetic drugs of abuse. ACS Chem Neurosci 4:1081–1092
31. Marshell R, Kearney-Ramos T, Brents LK, Hyatt WS, Tai S, Prather PL, Fantegrossi WE (2014) In vivo effects of synthetic cannabinoids JWH-018 and JWH-073 and phytocannabinoid Δ^9-THC in mice: inhalation versus intraperitoneal injection. Pharmacol Biochem Behav 124:40–47
32. Johansson E, Norén K, Sjövall J, Halldin MM (1989) Determination of Δ^1-tetrahydrocannabinol in human fat biopsies from marihuana users by gas chromatography–mass spectrometry. Biomed Chromatogr 3:35–38
33. Kreuz DS, Axelrod J (1973) Δ^9-tetrahydrocannabinol: localization in body fat. Science 179:391–393
34. Gunasekaran N, Long LE, Dawson BL, Hansen GH, Richardson DP, Li KM, Arnold JC, McGregor IS (2009) Reintoxication: the release of fat-stored Δ^9-tetrahydrocannabinol (THC) into blood is enhanced by food deprivation or ACTH exposure. Br J Pharmacol 158:1330–1337
35. Hasegawa K, Wurita A, Minakata K, Gonmori K, Nozawa H, Yamagishi I, Watanabe K, Suzuki O (2015) Postmortem distribution of AB-CHMINACA, 5-fluoro-AMB, and diphenidine in body fluids and solid tissues in a fatal poisoning case: usefulness of adipose tissue for detection of the drugs in unchanged forms. Forensic Toxicol 33:45–53
36. Takayama T, Suzuki M, Todoroki K, Inoue K, Min JZ, Kikura-Hanajiri R, Goda Y, Toyo'oka T (2014) UPLC/ESI-MS/MS-based determination of metabolism of several new illicit drugs, ADB-FUBINACA, AB-FUBINACA, AB-PINACA, QUPIC, 5F-QUPIC and alpha-PVT, by human liver microsome. Biomed Chromatogr 28:831–838
37. Watanabe K, Yamaori S, Funahashi T, Kimura T, Yamamoto I (2007) Cytochrome P450 enzymes involved in the metabolism of tetrahydrocannabinols and cannabinol by human hepatic microsomes. Life Sci 80:1415–1419
38. Kevin RC, Allsop DJ, Lintzeris N, Dunlop AJ, Booth J, McGregor IS (2017) Urinary cannabinoid levels during nabiximols (Sativex®)-medicated inpatient cannabis withdrawal. Forensic Toxicol 35:33–44